Free alternate bars in rivers: key physical mechanisms and simple formation criterion

Marco Redolfi[1]

[1]Department of Civil, Environmental and Mechanical Engineering, University of Trento, Italy.

Key Points:

- Essential features of alternate bars can be captured by neglecting the water surface deformation
- Free bars formation essentially depends on an imbalance between of water weight and bottom friction, which produces flow accelerations
- We derived and tested an explicit, physically based formula for predicting the occurrence of free migrating bars in rivers

Corresponding author: Marco Redolfi, `marco.redolfi@unitn.it`

Abstract

Free alternate bars are large-scale, downstream-migrating bedforms characterized by an alternating sequence of three-dimensional depositional fronts and scour holes that frequently develop in rivers as the result of an intrinsic instability of the erodible bed. Theoretical models based on two-dimensional shallow water and Exner equations have been successfully employed to capture the bar instability phenomenon, and to estimate bar properties such as height, wavelength and migration rate. However, the mathematical complexity of the problem hampered the understanding of the key physical mechanisms that sustain bar formation. To fill this gap, we considered a simplified version of the equations, based on neglecting the deformation of the free surface, which allows us to: (i) provide the first complete explanation of the bar formation mechanism as the result of a simple bond between variations of the water weight and flow acceleration; (ii) derive a simplified, physically based formula for predicting bar formation in a river reach, depending on channel width-to-depth ratio, Shields number and relative submergence. Comparison with an unprecedented large set of laboratory experiments reveals that our simplified formula appropriately predicts alternate bar formation in a wide range of conditions. Noteworthy, the hypothesis of negligible free surface effect also implies that bar formation is fully independent of the Froude number. We show that this intriguing property is intimately related to the three-dimensional nature of river bars, which allows for a gentle lateral deviation of the flow without significant deformation of the water surface.

1 Introduction

Alternate bars are characterized by a sequence of large-scale deposition bumps and scour holes that occupy alternate sides of the channel, showing diagonal fronts as in the example of Figure 1. The formation of alternate bars in rivers is important from an engineering perspective, as they can affect navigability, enhance bank erosion and interact with instream engineering structures [e.g. *Claude et al.*, 2014]. Moreover, bar formation represents a fascinating example of self-sustained morphodynamic process, which has been considered a precursor for the formation of river meandering and braiding [e.g., *Fredsoe*, 1978], and a main driver for channel widening [e.g. *Repetto et al.*, 2002] and for the formation of channel bifurcations [e.g, *Redolfi et al.*, 2016].

A large number of laboratory experiments demonstrated that downstream-migrating alternate bars tends to spontaneously form in straight channels of constant width [e.g. *Jaeggi*, 1984; *Fujita and Muramoto*, 1982; *Ikeda*, 1984; *Lanzoni*, 2000; *Crosato et al.*, 2012; *Nelson and Morgan*, 2018; *Redolfi et al.*, 2020]. This kind of bars, often referred to as "free alternate bars", are frequently observed in rivers [e.g. *Jaballah et al.*, 2015; *Rodrigues et al.*, 2015; *Adami et al.*, 2016; *Serlet et al.*, 2018; *Church and Rice*, 2009; *Ferguson et al.*, 2011], especially in channelized, gravel-bed rivers.

Two- and three-dimensional mathematical models have been employed to investigate different morphodynamic characteristics of free alternate bars, including: the effect of sediment heterogeneity [*Lanzoni and Tubino*, 1999; *Rodrigues et al.*, 2015; *Qian et al.*, 2017; *Cordier et al.*, 2019]; the effect of flow variability *Tubino* [1991]; *Hall* [2004]; the interaction between free and forced (or hybrid) bars [*Tubino and Seminara*, 1990; *Duró et al.*, 2016]; the effect of suspended sediment load [*Tubino et al.*, 1999; *Federici and Seminara*, 2006; *Bertagni and Camporeale*, 2018]; the transition from alternate bars to to three-dimensional oblique dunes [*Colombini and Stocchino*, 2012]; the morphodynamic effect of vegetation [*Bertagni et al.*, 2018; *Jourdain et al.*, 2020; *Caponi et al.*, 2019].

Mathematical modelling allowed for the identification of the essential processes needed to reproduce free bar formation. They revealed that three-dimensional effects

such as helical motion or flow separation are of secondary importance, so that the process of bar formation can be effectively predicted by means of depth-averaged, two-dimensional shallow water and Exner equations. Specifically, linear stability analyses [*Callander*, 1969; *Parker*, 1976; *Fredsoe*, 1978; *Colombini et al.*, 1987] demonstrated that even for a straight channel of constant width the basic, uniform-flow solution is inherently unstable, which leads from the spontaneous formation of long, three-dimensional bed deformations representing free alternate bars. Moreover, these theoretical analyses provided an useful criterion to determine marginal stability conditions, which are mainly controlled by the channel width-to-depth ratio. Specifically, bars are expected to form when the width-to-depth ratio exceeds a critical threshold that depends on other river characteristics (primarily relative roughness and Shields number).

Nevertheless, the mathematical complexity of the problem limited the derivation of explicit, physically based expressions for the critical aspect ratio as a function of the controlling parameters, as also recently highlighted by [*Crosato and Mosselman*, 2020]. As a consequence, application of the theory currently requires either to numerically solve a dispersion relation involving complex numbers, or to rely on plots made available by different authors, with limited possibility to explore the space of parameters and the effect of different transport and friction formulae. A possible alternative is based on empirical criteria proposed in the literature [e.g., *Muramoto and Fujita*, 1978; *Jaeggi*, 1984; *Yalin and Da Silva*, 2001; *Ahmari and Da Silva*, 2011]. Despite being originally formulated in different ways, empirical relations can be re-expressed in terms of the threshold value of the width-to-depth ratio that needs to be exceeded to enable the formation of bars. However, the empirical nature of these criteria makes it difficult to extend predictions out of the set of conditions for which they are derived. Moreover, empirical relations do not allow for isolating the effect of the individual physical parameters, and to assimilate information that may come from site-specific estimations of hydraulic roughness or sediment transport relations.

More fundamentally, the mathematical complexity highly limited the possibility to provide a satisfactory physical explanation of the mechanism of bar instability. A first tentative explanation was proposed by [*Einstein and Shen*, 1964], who suggested that bars may form as a consequence of helical motion, possibly reinforced by the presence of rough banks. However, subsequent models have conclusively demonstrated that neither three-dimensional flow nor rough banks are essential for capturing the bar instability mechanism. More recent explanations [*Nelson*, 1990; *Tubino et al.*, 1999] are given in terms of the divergence of the flow field around bars, due to a sort of topographic steering. However, the mechanism that produces this flow field has not been clarified. Therefore, a complete physical description of the instability process is essentially missing.

In this work, we consider a simplified version of the governing equations, in order to: (i) derive a simple, explicit expression for predicting bar stability conditions and validate it by means of existing laboratory experiments; (ii) provide a physically based explanation of the bar formation mechanism.

The paper is organized as follows: in Section 2 we define the governing equations and we specify the fundamental assumptions; in the Results Section 3 we introduce the simple criterion for predicting the formation of free alternate bars, we test it against existing laboratory data, and we provide a physical explanation of the bar formation mechanism; in Section 4 we discuss model hypotheses and associated limitations. Finally, details about the derivation of the explicit expression for the critical aspect ratio are reported in Appendix A .

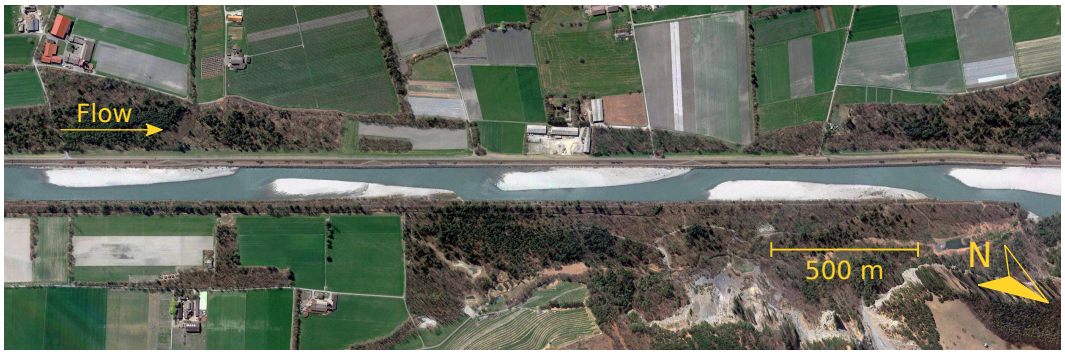

Figure 1: Example: downstream-migrating alternate bars in the Alpine Rhine River in Switzerland, $47°02' N$, $09°29' E$, 02-Apr-2012. From *Google Earth, Digital Globe (2021)*. Flow is from left to right.

2 Mathematical formulation

2.1 The governing equations

We consider an infinitely-long channel, with straight, fixed banks and rectangular cross-section of width W, whose bottom is formed by cohesionless particles with representative (e.g., median) grain size d. We adopt a two-dimensional, mobile-bed, depth-averaged shallow water model [e.g., *Parker*, 1976; *Colombini et al.*, 1987; *Siviglia et al.*, 2013], which can be written as a nonlinear differential system of four equations in the four dependent variables U, V, D and H (longitudinal and transverse velocity, water depth and water surface elevation), in the independent variables x, y (planimetric coordinates) and t (time). As sketched in Figure 2, the origin of the cartesian system of reference is positioned at the right bank, and elevations are calculated with respect to a sloping plane having longitudinal gradient S_0. Under quasi-steady approximation (i.e. assuming that the flow field adapts instantaneously to variations of the bed topography), the depth-averaged equations that express the conservation of momentum, liquid and solid mass read:

$$U\frac{\partial U}{\partial x} + V\frac{\partial U}{\partial y} - gS_0 + g\frac{\partial H}{\partial x} + \frac{\tau_x}{\rho D} = 0, \tag{1a}$$

$$U\frac{\partial V}{\partial x} + V\frac{\partial V}{\partial y} + g\frac{\partial H}{\partial y} + \frac{\tau_y}{\rho D} = 0, \tag{1b}$$

$$\frac{\partial UD}{\partial x} + \frac{\partial VD}{\partial y} = 0, \tag{1c}$$

$$(1-p)\frac{\partial \eta}{\partial t} + \frac{\partial qs_x}{\partial x} + \frac{\partial qs_y}{\partial y} = 0, \tag{1d}$$

where p is the sediment porosity, g is the gravitational acceleration, $\eta = H - D$ is the bed elevation, and the couples $\{\tau_x, \tau_y\}$ and $\{qs_x, qs_y\}$ indicate the components of the shear stress and the sediment transport, respectively.

The set of four differential equations is then completed by specifying closure relationships. Specifically, the two components of bed shear stress are estimated as follows:

$$\{\tau_x, \tau_y\} = \rho\frac{U^2}{c^2}\{\sin\gamma_q, \cos\gamma_q\}, \quad \tan\gamma_q = \frac{V}{U}, \tag{2}$$

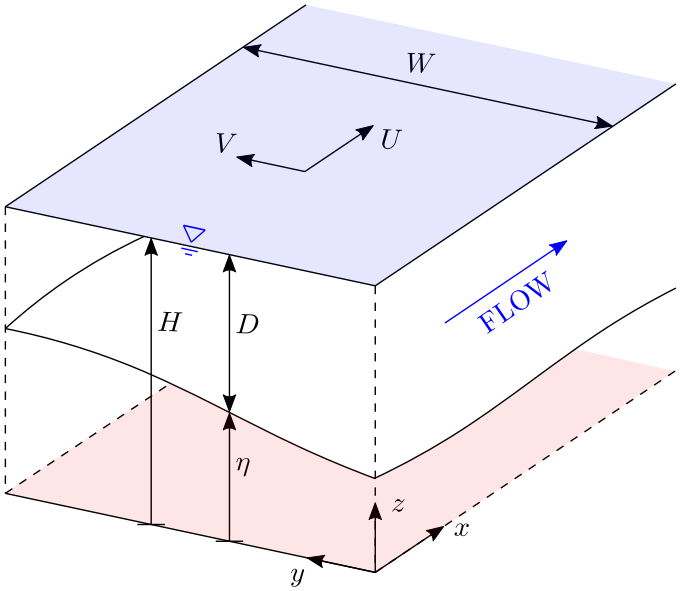

Figure 2: View of the channel of width W, showing the system of reference, $\{x, y, z\}$, and the two components of the velocity vector, $\{U, V\}$. The water surface elevation H is given by the sum of the bed elevation η and the water depth D. All the elevations are calculated with respect to the reference, $z = 0$, plane having a constant downstream gradient S_0.

where c is the dimensionless Chézy coefficient (a function of the relative submergence D/d) and γ_q is the angle of the velocity vector $\vec{U}$. The components of sediment transport are expressed as:

$$\{qs_x, qs_y\} = \sqrt{g\Delta d^3}\Phi(\theta)\{\sin\gamma_s, \cos\gamma_s\}, \tag{3}$$

where Δ is the relative submerged weight of the sediment and Φ is the dimensionless sediment flux, which is considered to be a function of the Shields number θ [e.g. *Meyer-Peter and Muller*, 1948; *Parker*, 1990]. The angle of the sediment transport vector, γ_s, is computed by taking into account the deflection exerted by the lateral bed slope, by means of the following expression [e.g., *Engelund*, 1981; *Blondeaux and Seminara*, 1985]:

$$\sin\gamma_s = \frac{qs_y}{|\vec{qs}|} = \sin\gamma_q - \frac{r}{\sqrt{\theta}}\frac{\partial\eta}{\partial y}, \tag{4}$$

where r is a dimensionless empirical coefficient [see *Baar et al.*, 2018].

Despite neglecting three-dimensional flow structures, this model has been proven to be able to capture the essential characteristics of river alternate bars, at least in conditions where most of the sediment is transported as bedload [e.g., *Blondeaux and Seminara*, 1985]. Specifically, linear solutions allow for calculating bar formation conditions, while weakly-nonlinear and fully nonlinear theories enable for reproducing bar height and to estimate other bar properties.

2.2 The key hypothesis

The present manuscript is founded on the key hypothesis that the deformation of the free surface due to the incipient formation of bars is negligible. More precisely, we assume that: (i) the pressure term $g\,\partial H/\partial x$ in the Equation of longitudinal momentum

(1a), and (ii) the variation of H when computing the bed elevation as $\eta = H - D$ in Equations (1d) and (4), are both negligible. It is worth noticing, however, that variations of the free surface elevation are still considered in the Equation of transverse momentum (1b), in which the pressure term $g\,\partial H/\partial y$ can not be disregarded.

This hypothesis has been used to model the formation of forced steady bars in rivers [e.g. *Struiksma et al.*, 1985; *Crosato and Mosselman*, 2009], and constitutes the basis for the so-called second order models for the evolution of meandering channels [see *Camporeale et al.*, 2007]. The appropriateness of adopting this hypothesis for modelling the evolution of free migrating bars is suggested by visual inspection of experimental data, where fluctuations are usually small, even at relatively high values of the Froude number *García and Niño* [1993]. Moreover, it is indirectly indicated by the weak dependence of alternate bars on Froude number [*Wilkinson et al.*, 2008], as characteristic of processes where the influence of free surface variations is small.

In the following Section 3, the comparison with the complete model and the validation against experimental data are used to demonstrate the suitability of this key hypothesis for predicting bar stability conditions. Moreover, in Section 4, we will discuss about the physical reasoning of why water surface deformation is negligible for typical hydrodynamic conditions on river bars.

2.3 Expression for the critical width-to-depth ratio

Neglecting the deformation of the free surface elevation allows for deriving an explicit formula for determining the possibility of migrating alternate bars to form, depending on channel characteristics and flow conditions. To this aim, we first need to specify a reference depth D_0 and the associated reference Shields number θ_0, which is given by the following uniform-flow relationship:

$$\theta_0 = \frac{S_0 D_0}{\Delta\, d}. \tag{5}$$

Bars formation primarily depends on the channel aspect ratio, which for historical reasons is here defined as *half* the width-to-depth ratio, namely:

$$\beta = \frac{W}{2D_0}. \tag{6}$$

Specifically, when the aspect ratio exceeds a critical threshold value (β_C) the initial, plane-bed configuration is unstable, and alternate bars are expected to spontaneously form [*Colombini et al.*, 1987].

A very simple formula for this critical aspect ratio can be obtained by: (i) linearizing the governing equations, (ii) considering the first mode of the Fourier expansion of the solution, (iii) analysing the time development of an initially-small bed perturbation, (iv) determining the set of parameters for which this initial perturbation tends to grow, eventually leading to finite-amplitude alternate bars. Considering that these mathematical procedure is rather standard and straightforward, we prefer avoid cluttering this section with a large number of equations. Therefore, we reported all the all the mathematical details in Appendix A , here providing only the final result of the linear stability analysis, which gives the following expression:

$$\beta_C = \frac{c_0}{2}\left[\frac{\xi(\theta_0)}{r}\,(1 + 2c_D) - \frac{1}{c_0^2\lambda^2}\right]^{-1/2}, \tag{7}$$

where the empirical coefficient r can be assumed equal to 0.3 and λ is the dimensionless wavenumber, defined as $\lambda = \pi W/L$, with L indicating the bar wavelength. Differently from the complete model of *Colombini et al.* [1987] our approach does not allow for estimating the bar wavenumber, which needs to be given as an input. However, considering a constant value $\lambda = 0.45$ is sufficient to produce accurate results for a range

of conditions. The symbol ξ indicates a function on the reference value of the Shields number (see Equation A.14b), which depends on the choice of the sediment transport formula. Specifically, considering the sediment transport formula of *Parker* [1978] it reads:

$$\xi(\theta_0) = \frac{\sqrt{\theta_0}}{\pi^2}\left(9\frac{\theta_{cr}}{\theta_0 - \theta_{cr}} + 2\right), \quad \theta_{cr} = 0.03. \tag{8a, b}$$

Similarly, the reference dimensionless Chézy coefficient c_0 and the associated c_D coefficient (Equation A.6b) depend on the choice of the friction formula. Adopting the widely-used logarithmic expression [*Engelund and Hansen*, 1967] gives:

$$c_0 = 6 + 2.5\log\left(\frac{1}{2.5}\frac{D_0}{d}\right), \quad c_D = \frac{2.5}{c_0}, \tag{9a, b}$$

where the ratio D_0/d represents the relative submergence. Alternatively, the friction coefficients can be calculated from the Manning formula as follows:

$$c_0 = \frac{D_0^{1/6}}{n\sqrt{g}}, \quad c_D = 1/6, \tag{10}$$

where the Manning coefficient n needs to be estimated on the basis of the bed roughness.

3 Results

3.1 Why do free bars form? A physical explanation

The hypothesis of negligible variations of the water surface elevation allows for a great simplification of the problem, as needed to physically understand the mechanisms that drive the formation and suppression of free alternate bars.

The bar-forming mechanism

We consider the depth-averaged Equation of the streamwise momentum (1a), where we neglect the transverse flux of longitudinal momentum (second term), as appropriate when studying the initial stages of bar development (see Appendix A):

$$U\frac{\partial U}{\partial x} = gS_0 - g\frac{\partial H}{\partial x} - \frac{\tau_x}{\rho D}. \tag{11}$$

By discarding the term related to the water surface deformation (i.e. according to our fundamental hypothesis), the above Equation (11), once multiplied by ρD, reads:

$$\underbrace{\rho U D\frac{\partial U}{\partial x}}_{\text{Inertia}} = \underbrace{\rho g D S_0}_{\text{Weight}} - \underbrace{\tau_x}_{\text{Friction}}, \tag{12}$$

which simply states that any imbalance between the longitudinal component of the water weight and the bottom friction necessarily produces a flow acceleration or deceleration.

In plane-bed conditions the flow is uniform, weight and friction keep in balance (i.e. $\tau_x = \rho g D S_0$) and no acceleration/deceleration occur. In this case, the sediment transport is also uniform, so that neither erosion nor deposition appear. Conversely, if a three-dimensional perturbation of the bed is introduced, the flow is no longer uniform. Let us consider for example a deposition bump at one side of the channel (i.e. a three-dimensional bed disturbance), having a length of several times the channel width and an initially-small height (Figure 3). Since the free surface deformation is negligible, the depth over the deposition bump does clearly reduce, and the weight of

the water column decreases. Considering that the friction term does not substantially change until the flow velocity varies (it is actually possible to assume τ_x to be constant, as discussed later), the decrease of weight does necessarily produce a flow deceleration ($\partial U/\partial x < 0$). This implies a spatial decrease in the sediment flux and an associated deposition, which increases the height of the initial bed disturbance. Similarly, a scour hole would produce an increase of depth and water weight, which in turn would lead to flow acceleration, spatial increase of sediment flux and further erosion. This represents a self-sustained instability mechanism, which ultimately leads to the formation of the large-scale, finite-amplitude bedforms called free bars.

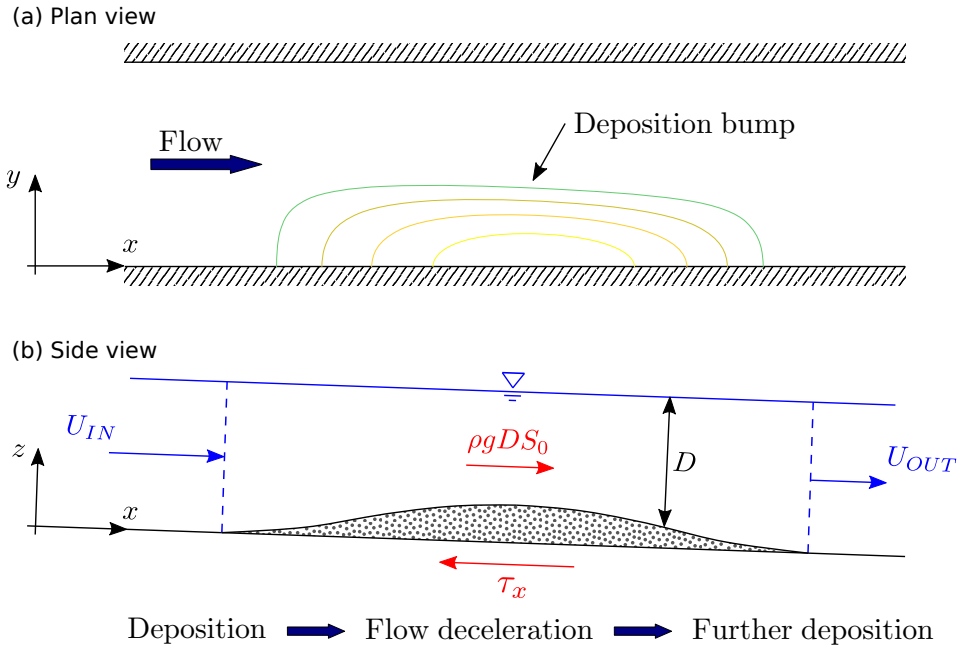

Figure 3: Illustration of the physical mechanism that sustains the bar growth. The generic, initially-small, three-dimensional deposition bump located near the right bank (see contour lines in the plan view) produces a decrease of the local water depth (D) and an associated reduction of tracting force due to the weight of the water column ($\rho g D S_0$). The imbalance between the reduced water weight and the bed friction τ_x necessarily produces a flow deceleration ($U_{OUT} < U_{IN}$), which induces further deposition, thus producing a self-sustained bar growth.

It is worth highlighting that the above-described mechanism is only valid for a three-dimensional bed perturbation, where the flow has enough space to move laterally around the obstacle without significant deformation of the free surface. Conversely, if the bed perturbation was purely two-dimensional, the flow would be obliged to entirely transit over the bedform, and the momentum balance would be affected by the pressure terms associated with the variations of the free surface. In these conditions, the shallow-water-Exner model invariably gives a suppression of the perturbation, which indicates that the basic uniform flow is always stable.

The bar-suppressing mechanism

The main contrasting mechanism is due to the gravitational effect on the direction of the bedload transport: the sediment tends to be deviated by an angle γ_s that depends on the lateral slope according to Equation (4). As illustrated in Figure 4

this deviation produces a transverse sediment flux towards the lower part of the cross-section (bar pools). This mechanism tends to suppress three-dimensional bedforms, eventually leading to flat-bed conditions if no other, constructive forces exist.

Specifically, the transverse flux of sediment (qs_y) predicted by Equation (4) is proportional to the lateral slope $\partial\eta/\partial y$. This represents the characteristic relation of diffusive processes, where the mass flux depends on the gradient, and is directed in the opposite direction [e.g., *Crank*, 1979]. As any diffusive process, the bed adaptation follows a timescale that is proportional to the square of the domain size (i.e. $T \propto W^2$). For example, considering a purely transverse bed deformation (no variations along the longitudinal direction - no constructive forces) the time needed to attain flat-bed conditions is proportional to the square of the channel width. This indicates that the bar-suppressing mechanism is more intense in relatively narrow channels, which justifies the presence of a lower threshold of the channel aspect ratio (β_C). More precisely, this explains why an exponent $-1/2$ appears in the expression for the critical aspect ratio (7) (i.e. the stability condition depends on the square of β, see also Equation (A.14a)).

In physical terms, this quadratic dependence can be easily understood by considering that channel width has a twofold effect. First, transverse bed gradient and the associated transverse flux of sediment are inversely proportional to the channel width. Second, the volume of sediments that needs to be laterally transferred is proportional to the width itself. Consequently, bed flattening in wider channel needs a larger mass transfer with a lower flux, therefore requiring a much longer time.

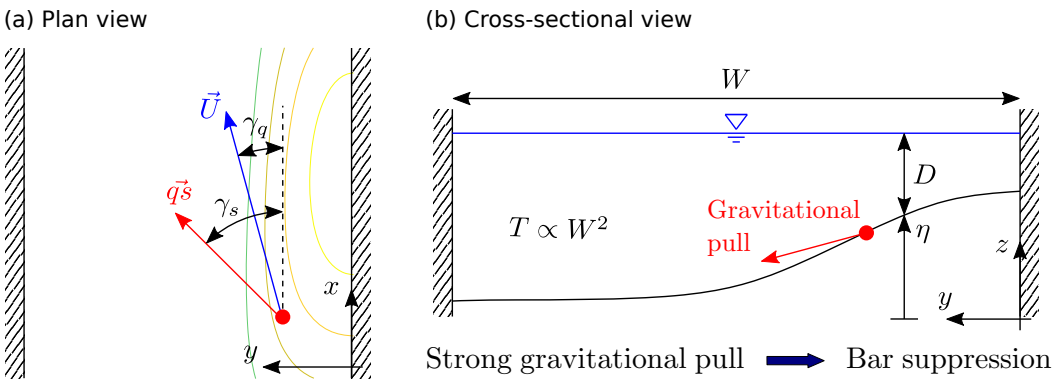

Figure 4: Effect of the gravitational pull on a laterally-sloping bed, which produces a downward deviation of the sediment flux $\vec{qs}$ with respect to the flow velocity vector $\hat{U}$ as illustrated in the plan view (a). As a result, the sediment flux tends to laterally move towards the most depressed areas, as illustrated in the cross-sectional view (b), which tends to flatten the bed. The timescale of the bed adaptation (T) is proportional to the square of the channel width (W) as typical of diffusive processes, which makes the bar-suppressing mechanism much more effective in relatively narrow channels.

3.2 When do free bars form? Results from the simplified criterion

The explicit expression for the critical aspect ratio (7) derived above provides a simple criterion for bar formation. Specifically, migrating alternate bars are predicted to form when the aspect ratio β exceeds the critical threshold β_C, while in the opposite case plane-bed conditions are expected, despite the possible development of low-relief oblique dunes [e.g., *Redolfi et al.*, 2020] or other kind of small-scale bedform.

As illustrated in Figure 5, the critical aspect ratio initially increases with the Shields number while it tends to slightly decrease when θ_0 exceeds 0.21, value at which the function $\xi(\theta_0)$ is minimum. Moreover, β_C significantly increases for higher values of the relative submergence, which according to Equation (9a) are associated with higher values of the Chézy coefficient c_0. In general, predictions by our simplified expression are very similar to those resulting from the complete model of *Colombini et al.* [1987]. Specifically, the critical aspect ratio shows a maximum relative error of 2.8% (for relatively high θ_0 and the low D_0/d), which seems acceptable for most applications.

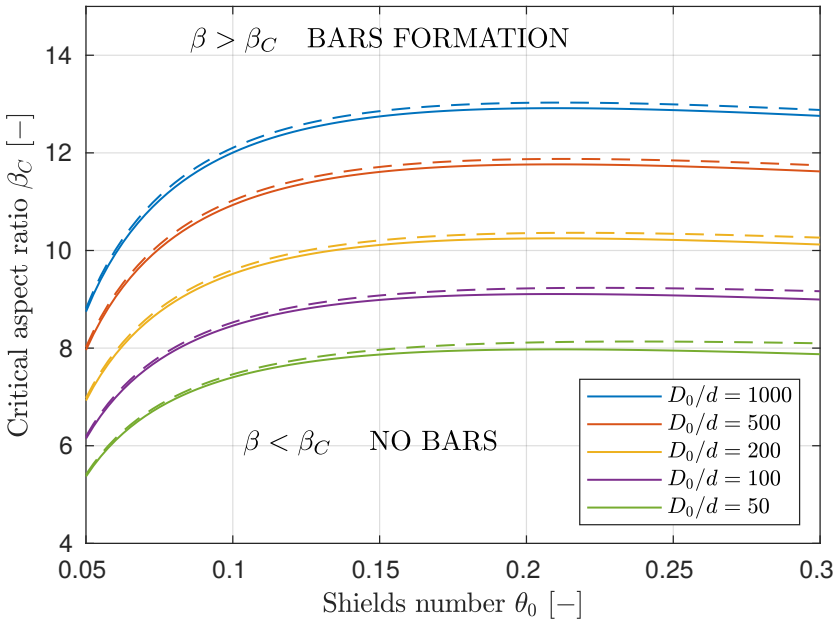

Figure 5: Critical aspect ratio resulting from the complete model of *Colombini et al.* [1987] (dashed lines) and by Equation (7) (solid lines), depending on Shields parameter (θ_0) and relative submergence (D_0/d). Migrating alternate bars are expected to form when the channel aspect ratio $\beta = W/(2D_0)$ exceeds the critical threshold β_C. The maximum relative error of the simplified model is 2.8%, which reduces to 1.6% when limiting the space of parameters to cases where the Froude number is lower than 1.

A further simplification can be obtained by neglecting the term $1/(c_0^2\lambda^2)$ in Equation (7), which gives a wavelength-independent stability condition. From a physical point of view, this means discarding the effect of velocity variations on the bed shear stress τ_x. If compared with the complete model of *Colombini et al.* [1987] this further reduced model leads to a maximum relative error of 4.5% within the range of parameters of Figure 5, which reduces to 3.2% when focussing on $Fr < 1$ cases only. Ultimately, a maximal simplification arises when considering also $c_D = 0$, which implies assuming spatially invariant bed shear stress (i.e. $\tau_x = const$). Though this may appear as an extreme hypothesis, it actually leads to an maximum relative error of about 16% with respect to the complete model, which indicates that variations of the shear stress play a secondary role in the above-described bar instability mechanism.

Comparison against experimental data

Comparison between our formula and experimental data is performed by considering the dataset reported by *Colombini et al.* [1987], encompassing experimental data from *Kinoshita* [1961]; *Ashida and Shiomi* [1966]; *Chang et al.* [1971]; *Sukegawa* [1971]; *Muramoto and Fujita* [1978]; *Ikeda* [1982]; *Jäggi* [1983] here expanded by including the more recent laboratory experiments by *García and Niño* [1993]; *Lanzoni* [2000]; *Ahmari and Da Silva* [2011]; *Crosato et al.* [2011]; *Garcia Lugo et al.* [2015]; *Redolfi et al.* [2020], for a total of 416 experiments. The formation of alternate bars was observed in 288 cases, where in the remaining 128 either plane bed or other bedforms (dunes, antidunes or diagonal bars) were observed.

As illustrated in Figure 6 our simple formula is able to correctly classify most of the experimental outcomes, as most of the experiments with alternate bars fall in the region $\beta > \beta_C$ while the remaining cases are often characterized by $\beta < \beta_C$. More specifically, 364 experiments (87.5%) are correctly classified, 35 (8.4%) can be designated as "false negative" (bars are observed to form, despite $\beta < \beta_C$) and 17 (4.1%) "false positive" (bars do not develop, despite $\beta > \beta_C$). It is worth highlighting that this result is obtained without any specific calibration of the empirical coefficient r or distinct choice of the sediment transport formula. In this sense, additional information about the sediment transport (e.g., measured transport rate) would enable for specifically calibrating the model parameters for each set of experiments, which is expected to improve the overall accuracy of the predictions.

The capability of Equation 7 to reproduce experimental results is then compared with analogue results from the application of the complete model and of the empirical criteria by *Muramoto and Fujita* [1978], *Jaeggi* [1984], *Yalin and Da Silva* [2001] and *Ahmari and Da Silva* [2011], whose expressions are reported in Appendix B . To this aim we first consider classic indicators of classification performance, namely the accuracy (ACC) and the balanced accuracy (BA) [see *Tharwat*, 2018], which are defined as follows:

$$ACC = \frac{N_{TP} + N_{TN}}{N_{tot}}, \quad BA = \frac{1}{2}\left(\frac{N_{TP}}{N_{TP} + N_{FN}} + \frac{N_{TN}}{N_{TN} + N_{FP}}\right), \tag{13a, b}$$

where N indicates the number of true positive (TP), true negative (TN), false positive (FP) and false negative (FN) cases, whose sum equals the total number of cases N_{tot}. We considered all the experimental data, except those having a severely limited bed mobility, due to low Shields number ($\theta_0 < 0.03$) or bed armouring. Results reported in Table 1 suggest that our formula gives essentially the same performance as the complete model of *Colombini et al.* [1987], which is overall better with respect to the other empirical criteria.

The above accuracy indicators are merely based on a binary (bars-no bars) classification but do not take into account the "degree of stability" predicted by the different cases. For example, experiments that are very close to the threshold are expected to be easily misclassified, so that an error in this case is less important that an error occurring in highly stable or unstable conditions. To overcome this limitation, we propose an indicator that accounts for the (logarithmic) distance of the incorrectly classified measurements from the critical threshold:

$$Dev = \frac{\sum_{\{FP,FN\}} |\log(\beta/\beta_C)|}{\sum |\log(\beta/\beta_C)|}, \tag{14}$$

where FP and FN indicate the set of false positive and false negative results, so that the parameter *dev* ranges from zero to one, with lower values indicating a good prediction. The observed values reported in Table 1 show that our formula provides similar results as the complete model of *Colombini et al.* [1987], with significantly less deviation than the other existing criteria.

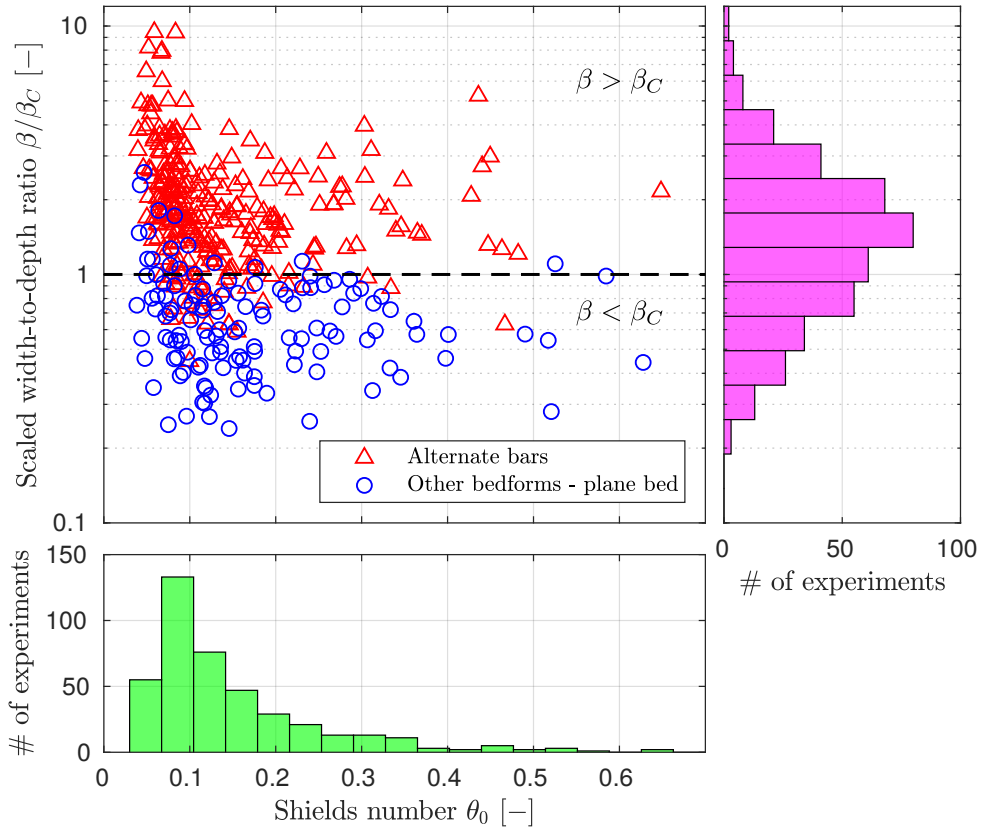

Figure 6: Comparison between our bar formation criterion and the dataset of laboratory experimental observations. Red triangles indicate conditions at which alternate bars were observed, while blue circles refers to other bed configurations, including plane-bed, diagonal bars, dunes and antidunes. Free alternate bars are expected to form when points fall above the dashed line that indicates the critical aspect ratio β_C. The histograms represent the frequency distribution of the experiments depending on Shields number (lower plot) and scaled width-to-depth ratio β/β_C (right plot).

Table 1: Classification performance of different bar predictors. *ACC* and *BA* indicate accuracy and balanced accuracy (Equations (13)a,b), while *Dev* is the indicator defined by Equation (14).

	ACC	*BA*	*Dev*
Muramoto and Fujita [1978]	83.2%	86.1%	8.1%
Jaeggi [1984]	80.3%	82.3%	15.8%
Yalin and Da Silva [2001]	77.4%	64.6%	11.8%
Ahmari and Da Silva [2011]	75.2%	61.3%	11.7%
Colombini et al. [1987]	87.0%	87.2%	5.2%
Present formula (7)	87.5%	87.3%	5.0%

4 Discussion

In this work we provide a novel explanation of the physical mechanism that leads to the spontaneous formation of free alternate bars in rivers. Surprisingly, this mechanism turns out to be extremely simple, to the point that it can be described as an imbalance between water weight and bottom friction, which causes deceleration near the top of bars and consequent further deposition. Specifically, the analysis of the two-dimensional solution of the shallow water model is to some extent simpler than its one-dimensional counterpart, as in the latter pressure terms due to the water surface deformation are rarely negligible. The bar formation is clearly counteracted by the effect of the lateral slope on the sediment transport, which tends to suppress bars [*Fredsoe*, 1978; *Seminara*, 2010]. In this perspective, our analysis highlights the strong (i.e. quadratic) dependence of this effect on the channel width, which represents the hallmark of diffusive processes.

Neglecting variations of the free surface elevation allows for obtaining an explicit expression for calculating the critical width-to-depth ratio with an error of a few percent with respect to the complete model of *Colombini et al.* [1987]. Comparison with an unprecedented number of laboratory experiments, encompassing more than 400 experimental runs from the existing literature, reveals that our explicit formula enables prediction of the bar formation in the vast majority of cases. Specifically, the resulting accuracy is comparable to that of the complete model and better with respect to existing empirical criteria. It is not our intention here to discuss what is the best criteria, as the answer is likely to depend on the specific objective of the analysis, on the availability of data and on the field of application. However, we find relevant to here highlight the main strengths of physically based expressions, which are directly derived from the equations of Newtonian mechanics through well-defined and testable assumptions. Following this reductionist approach [see *Seminara and Bolla Pittaluga*, 2012], the effect of all the essential parameters, including those that are normally fixed (e.g., the gravitational acceleration) is embodied, and can be directly associated with the underlying physical processes. In particular, our derivation allows for clarifying the following effects:

- the decrease of the critical aspect ratio for lower values of the relative submergence D_0/d (i.e. for low values of the Chézy parameter c_0) can be mechanically explained by considering that to maintain comparable values of Shields number and water depth on a rougher bed, weight and bottom friction need to be higher (i.e. the slope must be higher). In such conditions, any imbalance between the two terms on the right hand side of Equation (12) is expected to produce a stronger accelerations/decelerations, which reinforces the bar-forming mechanism;
- the Shields number shows two distinct and opposite effects. On the one side, increasing θ_0 makes the bar-forming mechanism less effective, as it reduces the sensitivity of the sediment transport to variations of velocity (i.e. the coefficient Φ_T, see Appendix A). On the other side, increasing θ_0 weakens the bar-suppressing mechanism, as it reduces the deflection of the sediment transport predicted by Equation 4. While the former effect dominates at moderate values of the Shields number, the latter prevails when $\theta_0 > 0.21$, which explains the non-monotonic trend of β_C appearing in Figure 5;
- higher values of the empirical parameter r enhance the bar-suppressing mechanism, as they are associated with a stronger deflection of the sediment transport (see again Equation (4)). Therefore, the critical aspect ratio clearly increases with r.

Knowing the effect of all the individual parameters allows for adapting the formula to the specific sediment transport and flow friction conditions, by assimilating information

from measurements or antecedent studies. For example, if field calibrated values of the Manning coefficient are available it is possible to bypass Equation (9a), and to directly compute c_0 from the Manning coefficient. This may be particularly important for the design and the interpretation of numerical simulations, as in this case our formula can be adapted to consider the same friction and sediment transport formulas, and exactly the same value of the parameter r.

4.1 The key hypothesis: physical reasoning and limitations

The appropriateness of neglecting free surface deformation is evident from the comparison between results of the simplified and the complete model illustrated above. However, here we would like to analyse the reason for which this hypothesis can be accepted, depending on the characteristic scales of the problem. A reader who is not interested to deepen this topic can directly jump to Section 4.2.

The validity of this hypothesis for modelling forced bars has been justified by *Struiksma et al.* [1985] by considering that when the Froude number is small, variations of the free surface elevation are small with respect to variations of the bed elevation. In these conditions it is possible to introduce the so-called rigid-lid assumption, which allows for computing variations of water depth on the basis of variations of the bed topography. However, this does not explain why variations of the free surface elevation can be neglected from the longitudinal momentum balance (1a), as the term $g\,\partial H/\partial x$ generally remains finite when $Fr \to 0$, representing the pressure gradient that appears under the rigid-lid assumption. For this reason, we found important to further discuss the possibility to neglect this term when modelling both free migrating bars (present paper) and forced (or hybrid) bars [*Crosato and Mosselman*, 2009; *Camporeale et al.*, 2007].

Here we show that this simplification is generally valid for the case of three-dimensional bed deformations having a longitudinal scale of several channel widths, as typically the case of all river alternate bars. Though this can be demonstrated by a mathematically rigorous perturbation approach, an analogous result can be found by simply evaluating the order of magnitude of the main terms of the fundamental conservation equations. Specifically, if we denote with $\tilde{D}$ and $(\tilde{U}, \tilde{V})$ the order of magnitude of the depth and velocity components, the continuity Equation (1c) gives:

$$\frac{\tilde{V}\tilde{D}}{\Delta\tilde{y}} \sim \frac{\tilde{U}\tilde{D}}{\Delta\tilde{x}}, \tag{15}$$

where $\Delta\tilde{x}$ and $\Delta\tilde{y}$ are the longitudinal and the transverse scales of variation. Indicating with Λ the ratio $\Delta x/\Delta y$, Equation (15) can be expressed as:

$$\tilde{V} \sim \frac{\tilde{U}}{\Lambda}, \tag{16}$$

which reveals that the magnitude of the transverse velocity decreases with the longitudinal scale.

The Equation of transverse momentum (1b) suggests that transverse acceleration and lateral inclination of the free surface have the same order magnitude, namely:

$$g\frac{\Delta\tilde{H}}{\Delta\tilde{y}} \sim \tilde{U}\,\frac{\tilde{V}}{\Delta\tilde{x}}, \tag{17}$$

where $\Delta\tilde{H}$ indicates the order of magnitude of the free surface variations. Combining Equations (17) and (16) gives:

$$g\frac{\Delta\tilde{H}}{\Delta\tilde{x}} \sim \tilde{U}\,\frac{\tilde{V}}{\Delta\tilde{x}}\frac{1}{\Lambda} \sim \tilde{U}\frac{\tilde{U}}{\Delta\tilde{x}}\frac{1}{\Lambda^2}, \tag{18}$$

which implies that the gravitational term in the Equation of longitudinal momentum (1a) is negligible when Λ is sufficiently large. The above condition (18) can be equivalently expressed in the Froude number as follows:

$$\frac{\Delta\tilde{H}}{\tilde{Fr}^2\tilde{D}} \sim \frac{1}{\Lambda^2}, \quad \tilde{Fr}^2 = \frac{\tilde{U}^2}{g\tilde{D}}, \tag{19a, b}$$

To test this conclusion we consider a periodic, double-sinusoidal bed deformation of amplitude A and wavelength L (Figure 7a). In this case the longitudinal and transverse scales of variations ($\Delta\tilde{x}$ and $\Delta\tilde{y}$) can be quantified as the distance between wave crest and trough ($L/2$ and W), so that their ratio Λ is given by $L/(2W) = \pi/(2\lambda)$. We then computed the two-dimensional flow field by analytically solving Equations (1a,b,c) under the hypothesis of small perturbations (linear analysis), by varying the wavelength of the bed oscillation (L) and the Froude number Fr, keeping all the other flow parameters invariant. Results illustrated in Figure 7 confirm that when increasing the value L/W (i.e. the value of Λ) transverse velocity and variations of the water surface elevation decrease, as predicted by Equations (16) and (19a). Moreover, for characteristic wavelengths of free migrating bars (L/W from 5 to 12, with typical value around 7, corresponding to $\lambda = 0.45$) and forced bars ($L/W > 12$) the complete solution is nearly independent of the Froude number, and is correctly reproduced by the simplified model, which corroborates the hypothesis of negligible free surface deformation.

This explains why alternate bars are essentially independent of the Froude number, to the point that they are weakly sensitive to the transition from sub- to supercritical flow regimes [*Wilkinson et al.*, 2008]. In this perspective, it is interesting to notice that this property has been recently observed by *Ragno et al.* [2021] for bifurcation-confluence loops, where the river splits in two anabranches than then rejoin downstream. This suggests that the weak dependence on the Froude number may represent a rather general, remarkable property of three-dimensional morphodynamic systems, such as multi-thread braided rivers, where the water flow is free to laterally move across bars and among different anabranches.

Similarly, the present analysis justifies why shorter three-dimensional bedforms like oblique dunes or diagonal bars [see *Colombini and Stocchino*, 2012] are instead significantly influenced by the Froude number. This is also the case of two-dimensional bed deformations, for which the independence of the Froude number is achieved only when the length scale of the bed slope variations is longer than the length of the backwater profiles (i.e. the so-called backwater length), so that the flow inertia is negligible and the morphological evolution is essentially diffusive [e.g., *Paola*, 2000; *Redolfi and Tubino*, 2014; *Shaw and McElroy*, 2016].

Ultimately, this analysis reveals that the model simplification adopted in this manuscript is possible thanks to the peculiar characteristic of bars being long, three dimensional bedforms, which allows the flow to deflect around bars without producing significant deformation of the water surface, even at moderate Froude numbers. For this reason, this hypothesis is usually not satisfied for two-dimensional bed deformations, for which the flow is obliged to surmount the bedforms, thus producing mechanically significant variations of the free surface.

4.2 Limitations and future perspectives

This work demonstrates that neglecting variations of the free surface elevation allows for a satisfactory prediction of the formation of free bars. However, it is worth highlighting that, differently from the complete linear theories [e.g. *Colombini et al.*, 1987], our model does not enable to determine the bar wavelength, because it predicts a monotonically-increasing instability for decreasing bar wavelength. This is clearly

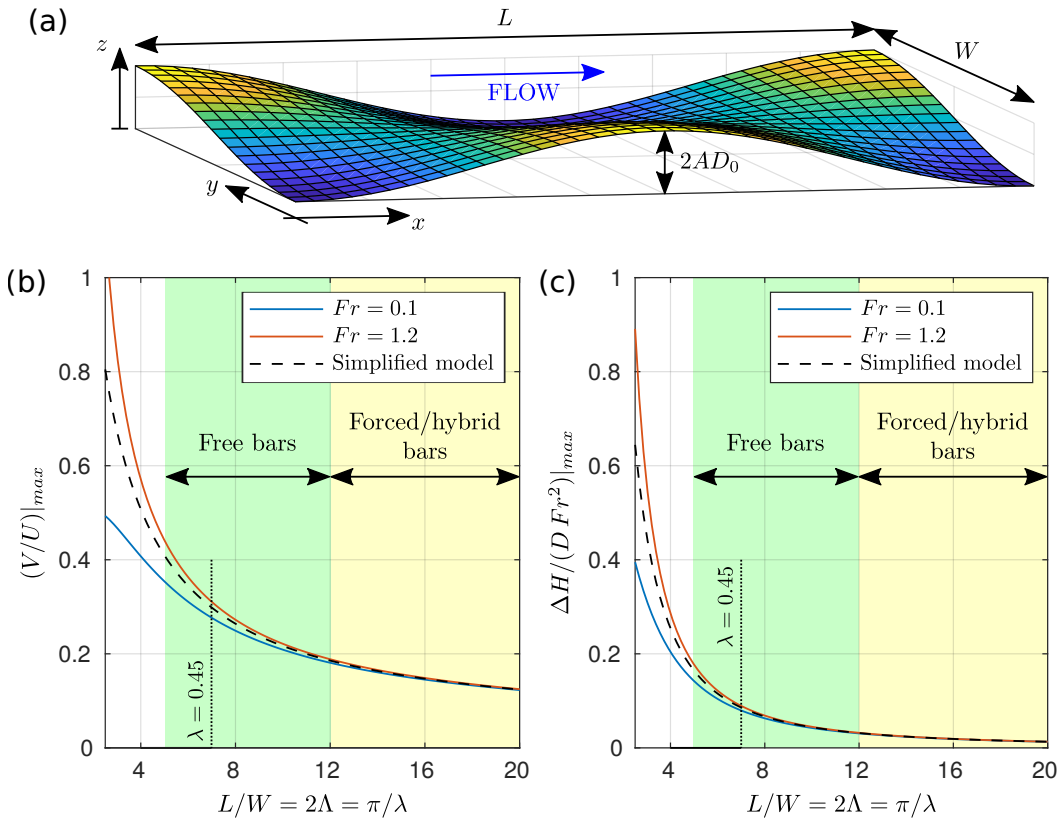

Figure 7: Effect of the bar wavelength on transverse velocity (V) and water surface deformation (ΔH), obtained by imposing a double-sinusoidal bed deformation of dimensionless amplitude A and wavelength L (a), and solving the linearized shallow water equations. Specifically, panels (b) and (c) report maximum values of V/U and $\Delta H/(Fr^2 D)$ for increasing values of L/W, considering an unitary dimensionless amplitude and two extreme values of the reference Froude number Fr. The solid lines refer to the complete linear solution, while the dashed line indicates the (Froude-independent) solution from our simplified model. For the typical wavelength of both free and forced/hybrid bars (shaded areas) the three lines tend to converge, which indicates the appropriateness of the fundamental hypothesis. The dotted line indicates the typical wavenumber $\lambda = 0.45$ we adopted when applying Equation (7). Example with $\beta = 12$ and $D_0/d = 100$.

related to the fact that, as demonstrated in Section 4.1, the key assumption is not valid for relatively short wavelengths. However, this limitation does not prevent for an accurate prediction of the critical aspect ratio, for two reasons: (i) the wavenumber resulting from complete theories is relatively constant, so that its average value $\lambda = 0.45$ can be considered representative; (ii) the critical aspect ratio resulting from Equation (7) is weakly sensitive to variations of the wavenumber, to the point that even setting $\lambda \to \infty$ (i.e. neglecting the term $1/(c_0^2\lambda^2)$) gives an error of a few percent only.

Our expression for the marginal stability condition is meant for predicting the formation of alternate (i.e first mode) bars only, and does not provide indications about the transition to higher bar modes (i.e. central or multiple-row bars) that is expected in wider channels [*Fredsoe*, 1978; *Crosato and Mosselman*, 2009]. Our approach could be easily extended to predict the growth rate of higher modes, which would allow us to determine the most unstable bar mode depending on conditions [see *Tubino et al.*, 1999]. However, this clearly goes beyond the purpose of the paper.

When applying our formula to rivers, the following question arises: "how to select an appropriate value of dominant, formative discharge that can be adopted to represent the bar response?". Previous works usually rely on either the bankfull discharge [e.g., *Crosato and Mosselman*, 2009; *Ahmari and Da Silva*, 2011; *Crosato and Mosselman*, 2020] or on the discharge with 2-year return period [e.g., *Adami et al.*, 2016], as commonly suggested for reproducing river morphodynamic processes. However, a specific methodology to derive formative conditions for migrating bars has been recently proposed by *Carlin et al.* [2021], who suggested that free bars are expected to form when the average growth rate, calculated over all the possible discharge states, is positive, namely:

$$\overline{\Omega} = \int_0^\infty \Omega \, f_Q \, dQ > 0, \tag{20}$$

where f_Q indicates the probability density function of the flow events. In this perspective, our analysis provides all the necessary information for directly computing the bar growth rate Ω as a function of discharge by means of Equation (A.13).

Finally, the present analysis is limited to conditions where most of the sediment is transported as bedload, as reproducing the effect of suspended load on bar stability requires a more sophisticated model, based on either a non-equilibrium stress-transport relation [*Federici and Seminara*, 2006; *Bertagni and Camporeale*, 2018] or on a fully three-dimensional approach [*Tubino et al.*, 1999]. However, our model allows for qualitatively explaining the increase of bar instability observed in suspension-dominated channels: since the suspended load is substantially not affected by the gravitational pull predicted by Equation (4), the bar-suppressing mechanism is expected to be weaker, which promotes bar formation.

5 Conclusions

Neglecting the deformation of the water surface in the classic two-dimensional shallow water and Exner model allowed for a considerable simplification of the mathematical description of the process of bar formation, which facilitated the physical understanding of the phenomenon. This led to the following conclusions:

- The physical mechanism that leads to a self-sustained development of free migrating bars is surprisingly simple, as it results from an imbalance between water weight and bottom friction. Specifically, if a relatively long, three-dimensional, deposition bump is introduced, water depth and associated weight reduce, which produces a flow deceleration and further deposition. The same but reversed mechanism occurs in three-dimensional pools, where the increase of water depth

produces acceleration and further scour. This bar-forming instability process tends to be counteracted by the effect of the gravitational pull on the bed particle transported as bed load. The importance of this bar-suppressing effect increases quadratically when reducing the channel width, which explains why bar formation is strongly discouraged when the channel width-to-depth ratio is low.

- An explicit, physically based formula for predicting conditions for the formation of free alternate bars can be derived. Testing based on a very large number of laboratory experiments, suggests that the formula we propose is on average more accurate than existing empirical predictors. Moreover, the physically based derivation of the formula allows for assessing the effect of all the essential parameters that concur in determining bar stability, and it is therefore suitable to be adapted and extended to a wide range of conditions.
- The hypothesis of negligible deformation of the water surface is intimately related to two essential characteristics of bars: (i) the three-dimensional structure; (ii) the long longitudinal extension, which allow for a gentle deviation of the flow, without significant variations of the water surface elevation. For this reason it does not apply to two-dimensional or comparatively short three-dimensional bedforms, such as two-dimensional dunes or oblique dunes. Ultimately, this hypothesis implies a that the Froude number plays a negligible role in the formation of bars. This suggests that a substantial independence of the Froude parameter may be a general, remarkable property of all morphodynamics systems characterized by a three-dimensional bed topography, such as multi-thread braided rivers.

Appendix A Derivation of an explicit expression for the critical aspect ratio

The linear stability analysis of the system of partial differential Equations (1) is obtained by considering small perturbations with respect to a reference, undisturbed flow, here denoted with the subscript $_0$. Specifically, we consider an expansion of the dependent variables in the form:

$$U = U_0\,[1 + U_1^*], \tag{A.1a}$$
$$V = U_0\,[0 + V_1^*], \tag{A.1b}$$
$$D = D_0\,[1 + D_1^*], \tag{A.1c}$$
$$H = D_0\,[0 + H_1^*], \tag{A.1d}$$

where $U_1^*, V_1^*, D_1^*, H_1^*$ represent the dimensionless perturbations.

Moreover, it is convenient to express also the independent variables in dimensionless form. Specifically, planimetric coordinates are scaled with half the channel width [*Colombini et al.*, 1987], namely:

$$x^* = \frac{x}{W/2}, \qquad y^* = \frac{y}{W/2}, \tag{A.2a, b}$$

while time is made dimensionless by means of the Exner timescale (i.e. that naturally arising from the sediment continuity equation), namely:

$$t^* = t\frac{qs_0}{(1-p)D_0W/2}. \tag{A.3}$$

Substituting the above expressions in the system of four differential Equations (1), considering the closure relations (2-4), and neglecting the nonlinear terms, gives

the following linear system:

$$\frac{\partial U_1^*}{\partial x^*} + \cancel{\frac{1}{Fr^2}\frac{\partial H_1^*}{\partial x^*}} + \frac{\beta}{c_0^2}\left[2U_1^* - D_1^*\left(1+2c_D\right)\right] = 0, \tag{A.4a}$$

$$\frac{\partial V_1^*}{\partial x^*} + \frac{1}{Fr^2}\frac{\partial H_1^*}{\partial y^*} + \frac{\beta}{c_0^2}V_1 = 0, \tag{A.4b}$$

$$\frac{\partial D_1^*}{\partial x^*} + \frac{\partial U_1^*}{\partial x^*} + \frac{\partial V_1^*}{\partial y^*} = 0, \tag{A.4c}$$

$$\frac{\partial(\cancel{H_1^*} - D_1^*)}{\partial t^*} + \frac{\partial V_1^*}{\partial y^*} - \frac{r}{\beta\sqrt{\theta_0}}\frac{\partial^2(\cancel{H_1^*} - D_1^*)}{\partial y^{*2}} + 2\Phi_T\frac{\partial U_1^*}{\partial x^*} - 2\Phi_T c_D\frac{\partial D_1^*}{\partial x^*} = 0, \tag{A.4d}$$

where the reference Froude number and aspect ratio are given by:

$$Fr = \frac{U_0}{\sqrt{gD_0}}, \qquad \beta = \frac{W/2}{D_0}. \tag{A.5a, b}$$

The dimensionless coefficients Φ_T and c_D, which measure the nonlinearity of the response of bedload and flow friction to variations of Shields number and water depth, are defined as:

$$\Phi_T = \frac{\theta_0}{\Phi_0}\frac{\partial\Phi}{\partial\theta}\Big|_{\theta=\theta_0}, \qquad c_D = \frac{D_0}{c_0}\frac{\partial c}{\partial D}\Big|_{D=D_0}, \tag{A.6a, b}$$

and their explicit expression depends on the choice of the sediment transport and friction formulae.

The spatial variations of the free surface elevations can be neglected from the water and sediment continuity equations, and from the longitudinal momentum equations (red-crossed terms). Conversely, they are still important to satisfy the equation of transverse momentum, as the water surface deformation is needed to guide the lateral flow movement. However, this simplification allows for decoupling the problem, as Equations (A.4a,c,d) can be resolved independently from Equation (A.4b). Moreover, isolating the term $\partial V_1/\partial y$ from the water continuity Equation (A.4c) and substituting it into the Exner Equation (A.4d) allows for reducing Equations (A.4a,c,d) into the following differential system of two equations in the two unknowns U_1 and D_1:

$$\frac{\partial U_1^*}{\partial x^*} + \frac{\beta}{c_0^2}\left[2U_1^* - D_1^*\left(1+2c_D\right)\right] = 0, \tag{A.7a}$$

$$-\frac{\partial D_1^*}{\partial t^*} - \frac{\partial D_1^*}{\partial x^*} - \frac{\partial U_1^*}{\partial x^*} + \frac{r}{\beta\sqrt{\theta_0}}\frac{\partial^2 D_1^*}{\partial y^{*2}} + 2\Phi_T\frac{\partial U_1^*}{\partial x^*} - 2\Phi_T c_D\frac{\partial D_1^*}{\partial x^*} = 0. \tag{A.7b}$$

Considering the simplified shallow water equations, we look for a wavelike solution where spatial variations assume the form of a double sinusoid as illustrated in Figure 7a. Specifically:

$$U_1^* = \hat{u}\exp\left[i\lambda x^* + (\Omega - i\omega)t^*\right]\cos(\pi y^*/2) + c.c., \tag{A.8a}$$

$$D_1^* = \hat{d}\exp\left[i\lambda x^* + (\Omega - i\omega)t^*\right]\cos(\pi y^*/2) + c.c., \tag{A.8b}$$

where $\hat{u}$ and $\hat{d}$ are complex coefficients, $i = \sqrt{-1}$ denotes the imaginary unit, *c.c.* indicates the complex conjugate. The real coefficients Ω and ω represent the dimensionless growth rate and angular frequency, while λ is the dimensionless longitudinal wavenumber, defined as $\lambda = \pi W/L$, where L is the bar wavelength.

Substituting Equations (A.8) into the system of linear Equations A.7 leads to a system of algebraic equations in the unknowns $\hat{u}$ and $\hat{d}$ that can be expressed in the following matrix form:

$$\begin{bmatrix} i\lambda + a_1 & a_2 \\ i\lambda(1-a_4) & i\lambda(1-a_5) + \pi^2/4\, a_6 + \Omega - i\omega \end{bmatrix} \times \begin{bmatrix} \hat{u} \\ \hat{d} \end{bmatrix} = \begin{bmatrix} 0 \\ 0 \end{bmatrix}, \tag{A.9}$$

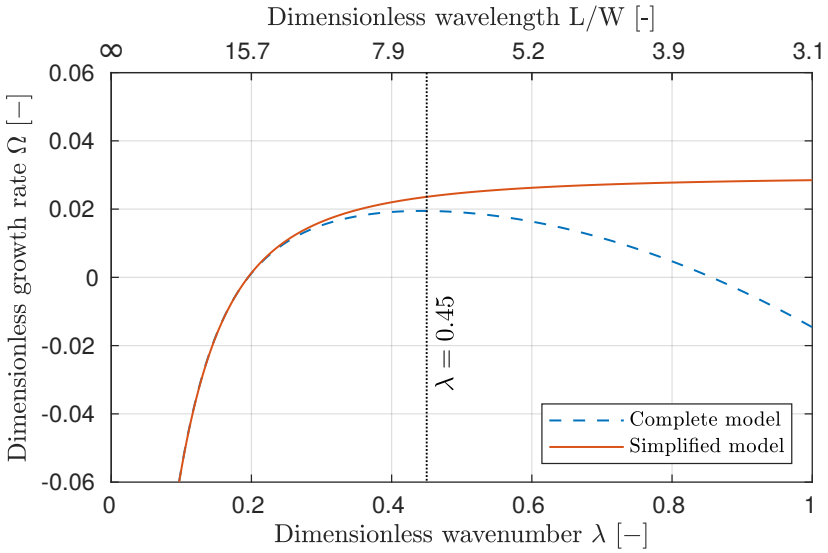

Figure A.1: Dimensionless growth rate as a function of the dimensionless wavenumber λ according to the complete model of [*Colombini et al.*, 1987] (dashed line) and our Equation A.13 (solid line). The above scale indicates the corresponding dimensionless wavelength L/W. The dotted line indicates the typical wavenumber $\lambda = 0.45$ we adopted when applying Equation (7). Example with $\beta = 10$, $\theta_0 = 0.1$ and $D_0/d = 200$.

where the "a" coefficients are defined as in *Camporeale et al.* [2007], namely:

$$a_1 = 2\beta/c_0^2, \quad a_2 = -(1+2c_D)\beta/c_0^2, \quad a_4 = 2\Phi_T, \quad a_5 = -2c_D\Phi_T, \quad a_6 = \frac{r}{\beta\sqrt{\theta_0}}. \quad \text{(A.10)}$$

A non-trivial solution of the homogeneous linear system (A.9) exists when the determinant of the matrix of coefficients vanishes, which gives:

$$\Omega - i\omega = -i\lambda(1-a_5) - \frac{\pi^2}{4}a_6 + a_2(1-a_4)\frac{i\lambda}{a_1+i\lambda}, \quad \text{(A.11)}$$

whose real part reads:

$$\Omega = -\frac{\pi^2}{4}a_6 + a_2(1-a_4)\frac{\lambda^2}{a_1^2+\lambda^2}, \quad \text{(A.12)}$$

which, substituting the coefficients (A.10), provides an expression for the bar growth rate Ω, namely:

$$\Omega = -\frac{\pi^2}{4}\frac{r}{\beta\sqrt{\theta_0}} + (1+2c_D)\frac{\beta}{c_0^2}(2\Phi_T - 1)\frac{\lambda^2}{4\beta^2/c_0^4+\lambda^2}. \quad \text{(A.13)}$$

As illustrated in Figure A.1 the resulting growth rate monotonically increases with the bar wavenumber λ. This prevents the possibility of determining the most unstable wavenumber, which needs to be provides as an input parameter. Considering the typical value $\lambda = 0.45$ the simplified model gives a growth rate that is similar to the maximum growth rate given by the complete model, which suggests its capability to correctly reproduce the formation of free alternate bars.

Marginal stability conditions are found by setting zero growth rate ($\Omega = 0$) in Equation (*A*.13), which gives:

$$\frac{4\beta_C^2}{c_0^2}\left[\frac{\xi(\theta_0)}{r}(1+2c_D) - \frac{1}{c_0^2\lambda^2}\right] = 1, \quad \xi(\theta_0) = \frac{\sqrt{\theta_0}}{\pi^2}(2\Phi_T - 1), \quad \text{(A.14a, b)}$$

from which it is easy to derive an explicit expression for the critical aspect ratio β_C.

Appendix B Critical aspect ratio according to empirical free bars predictors

In this section, we re-express existing empirical criteria in terms of the critical width-to-depth ratio, as needed for a direct comparison with our formula (7).

The criterion of *Muramoto and Fujita* [1978]

This criterion for the formation of free alternate bars can be written as [see *Jaeggi*, 1984]:

$$\frac{D_0/d}{(W/d)^{0.67}} < 0.45. \tag{B.1}$$

Once expressed in terms of the channel aspect ratio, Equation (B.1) reads:

$$\beta > \beta_C = \frac{1}{2}\,0.45^{-1/0.67}\left(\frac{D_0}{d}\right)^{1/0.67-1} = 1.647\left(\frac{D_0}{d}\right)^{0.493}, \tag{B.2}$$

which depends on the relative submergence D_0/d as illustrated in Figure B.1.

The criterion of *Jaeggi* [1984]

The bar formation criterion provided *Jaeggi* [1984] (see their Equation (8)), translated in our notation, reads:

$$\frac{\theta}{\theta_i} < 2.93\log\left(\frac{\theta}{\theta_i}\frac{W}{D}\right) - 3.13\left(\frac{W}{d}\right)^{0.15}, \tag{B.3}$$

which can be also rewritten in terms of the channel aspect ratio β as:

$$2.93\log\left(\frac{\theta}{\theta_i}2\beta\right) - 3.13\left(\frac{D_0}{d}2\beta\right)^{0.15} - \frac{\theta}{\theta_i} > 0. \tag{B.4}$$

Despite not allowing for deriving an explicit expression, Equation B.4 can be numerically solved to obtain the critical aspect ratio β_C.

However, it is worth highlighting that a critical aspect ratio does not always exist. This can be noticed by analyzing the left hand side of the inequality (B.4), which does not increase monotonically with β but it shows a maximum when:

$$\beta = k\,\frac{d}{D_0}, \quad k = \frac{1}{2}\left(\frac{2.93}{3.13\cdot 0.15}\right)^{1/0.15} = 1.00\cdot 10^5. \tag{B.5a, b}$$

A critical value of the aspect ratio exists only if the maximum value is positive, as given by substituting (B.5a) into (B.4):

$$2.93\log\left(\frac{\theta}{\theta_i}2k\frac{d}{D_0}\right) - \frac{2.93}{0.15} - \frac{\theta}{\theta_i} > 0, \tag{B.6}$$

which can be expressed in terms of the relative submergence as follows:

$$\frac{D_0}{d} < \frac{\theta}{\theta_i}k_2\exp\left(-\frac{1}{2.93}\frac{\theta}{\theta_i}\right), \quad k_2 = 2k\exp\left(-\frac{1}{0.15}\right) = 254.5. \tag{B.7a, b}$$

For Shields numbers in the range $1-6$ times θ_i, as usually the case of gravel bed rivers at bankfull conditions [*Parker et al.*, 2007], Equations (B.7) give minimum values of D_0/d between 181 and 274. For higher relative submergence D/d, Equation (B.4) is never satisfied, which implies that bars are not expected to form regardless of the value of β (see Figure B.1). It is worth noticing, however, that this prediction seems essentially a mathematical artifact, as the empirical formula was derived from observations in conditions of relatively low submergence ($D_0/d < 30$).

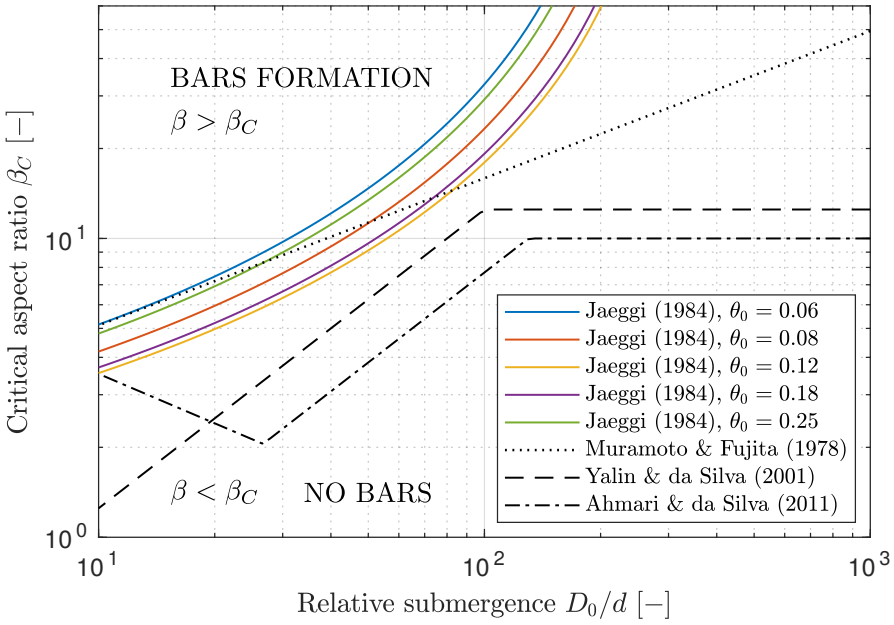

Figure B.1: Critical aspect ratio for the formation of free migrating bars according to the empirical criteria of *Muramoto and Fujita* [1978] (dotted line), *Jaeggi* [1984] (solid lines, depending on the Shields number θ_0), *Yalin and Da Silva* [2001] (dashed line) and *Ahmari and Da Silva* [2011] (dashed-dotted line). For all the criteria, bars are expected to form when the width-to-depth ratio exceeds the critical threshold.

The criterion of *Yalin and Da Silva* [2001]

This criterion is based on the empirical definition of a threshold value of the channel aspect ratio that only depends on the relative submergence (D_0/d). Specifically, it can be expressed by means on the following piecewise-linear function:

$$\beta_C = \begin{cases} \frac{1}{8}\frac{D_0}{d} & \text{if } \frac{D_0}{d} < 100 \\ 12.5 & \text{if } \frac{D_0}{d} >= 100 \end{cases}, \tag{B.8}$$

with alternate bars expected to form when $\beta > \beta_C$.

The criterion of *Ahmari and Da Silva* [2011]

This criterion can be regarded as an updated version of *Yalin and Da Silva* [2001], where the constant aspect ratio for high values of D_0/d is slightly reduced, and where a third branch of the solution is introduce to consider a decrease of the critical width-to-depth ratio for small values of the relative submergence. Specifically, the authors proposed the following piecewise-linear function:

$$\beta_C = \begin{cases} 12.5\left(\frac{D_0}{d}\right)^{-0.55} & \text{if } \frac{D_0}{d} < 26.69 \\ \frac{1}{13}\frac{D_0}{d} & \text{if } 26.69 <= \frac{D_0}{d} < 130 \\ 10 & \text{if } \frac{D_0}{d} >= 130 \end{cases}. \tag{B.9}$$

A comparison among the different expressions is illustrated in Figure B.1.

Acknowledgments

All experimental data are available at `https://bitbucket.org/Marco_Redolfi/free_bars_analysis`. I thank prof. Marco Tubino and prof. Walter Bertoldi for kindly providing data they previously collected and organized. This research has progressed in the author's spare time.

References

Adami, L., W. Bertoldi, and G. Zolezzi (2016), Multidecadal dynamics of alternate bars in the Alpine Rhine River, *Water Resources Research*, *52*, 8938–8955, doi:10.1002/2015WR018228.

Ahmari, H., and A. M. F. Da Silva (2011), Regions of bars, meandering and braiding in da Silva and Yalin's plan, *Journal of Hydraulic Research*, *49*(6), 718–727, doi:10.1080/00221686.2011.614518.

Ashida, K., and Y. Shiomi (1966), Study on the hydraulics behaviour of meander in channels, *Disaster Prevention Research Institute Annuals*, pp. 457–477.

Baar, A. W., J. de Smit, W. S. J. Uijttewaal, and M. G. Kleinhans (2018), Sediment Transport of Fine Sand to Fine Gravel on Transverse Bed Slopes in Rotating Annular Flume Experiments, *Water Resources Research*, *54*(1), 19–45, doi:10.1002/2017WR020604.

Bertagni, M. B., and C. Camporeale (2018), Finite amplitude of free alternate bars with suspended load, *Water Resources Research*, *54*, 9759–9773, doi:10.1029/2018WR022819.

Bertagni, M. B., P. Perona, and C. Camporeale (2018), Parametric transitions between bare and vegetated states in water-driven patterns, *Proceedings of the National Academy of Sciences*, *115*(32), 8125–8130, doi:10.1073/pnas.1721765115.

Blondeaux, P., and G. Seminara (1985), A Unified Bar Bend Theory of River Meanders, *Journal of Fluid Mechanics*, *157*, 449–470.

Callander, R. A. (1969), Instability and river channels, *Journal of Fluid Mechanics*, *36*(3), 465–480, doi:10.1017/S0022112069001765.

Camporeale, C., P. Perona, A. Porporato, and L. Ridolfi (2007), Hierarchy of models for meandering rivers and related morphodynamic processes, *Reviews of Geophysics*, *45*(1), 1–28, doi:10.1029/2005RG000185.

Caponi, F., A. Koch, W. Bertoldi, D. F. Vetsch, and A. Siviglia (2019), When Does Vegetation Establish on Gravel Bars? Observations and Modeling in the Alpine Rhine River, *Frontiers in Environmental Science*, *7*, 124, doi:10.3389/fenvs.2019.00124.

Carlin, M., M. Redolfi, and M. Tubino (2021), The Long-Term Response of Alternate Bars to the Hydrological Regime, *Water Resources Research*, *57*(7), doi:10.1029/2020WR029314.

Chang, H.-Y., D. B. Simons, and D. A. Woolhiser (1971), Flume experiments on alternate bar formation, *Journal of the Waterways, Harbors and Coastal Engineering Division*, *97*(1), 155–165.

Church, M., and S. P. Rice (2009), Form and growth of bars in a wandering gravel-bed river, *Earth Surface Processes and Landforms*, *34*(10), 1422–1432, doi:10.1002/esp.1831.

Claude, N., S. Rodrigues, V. Bustillo, J.-G. Bréhéret, P. Tassi, and P. Jugé (2014), Interactions between flow structure and morphodynamic of bars in a channel expansion/contraction, Loire River, France, *Water Resources Research*, *50*(4), 2850–2873, doi:10.1002/2013WR015182.

Colombini, M., and A. Stocchino (2012), Three-dimensional river bed forms, *J. Fluid Mech*, *695*, 63–80, doi:10.1017/jfm.2011.556.

Colombini, M., G. Seminara, and M. Tubino (1987), Finite-amplitude alternate bars, *Journal of Fluid Mechanics*, *181*(HY9), 213–232, doi:10.1017/S0022112087002064.

Cordier, F., P. Tassi, N. Claude, A. Crosato, S. Rodrigues, and D. Pham Van Bang (2019), Numerical Study of Alternate Bars in Alluvial Channels With Nonuniform Sediment, *Water Resources Research*, *55*(4), 2976–3003, doi:10.1029/2017WR022420.

Crank, J. (1979), *The mathematics of diffusion*, Oxford university press.

Crosato, A., and E. Mosselman (2009), Simple physics-based predictor for the number of river bars and the transition between meandering and braiding, *Water Resources Research*, *45*(3), 1–14, doi:10.1029/2008WR007242.

Crosato, A., and E. Mosselman (2020), An Integrated Review of River Bars for Engineering, Management and Transdisciplinary Research, *Water*, *12*(2), 596, doi:10.3390/w12020596.

Crosato, A., E. Mosselman, F. Beidmariam Desta, and W. S. J. Uijttewaal (2011), Experimental and numerical evidence for intrinsic nonmigrating bars in alluvial channels, *Water Resources Research*, *47*(3), W03511, doi:10.1029/2010WR009714.

Crosato, A., F. B. Desta, J. Cornelisse, F. Schuurman, and W. S. J. Uijttewaal (2012), Experimental and numerical findings on the long-term evolution of migrating alternate bars in alluvial channels, *Water Resources Research*, *48*(6), doi:10.1029/2011WR011320.

Duró, G., A. Crosato, and P. Tassi (2016), Numerical study on river bar response to spatial variations of channel width, *Advances in Water Resources*, *93*, 21–38, doi:10.1016/j.advwatres.2015.10.003.

Einstein, H. A., and H. W. Shen (1964), A study on meandering in straight alluvial channels, *Journal of Geophysical Research*, *69*(24), 5239–5247, doi:10.1029/jz069i024p05239.

Engelund, F. (1981), The motion of sediment particles on an inclined bed, *Progress Rep*, *53*.

Engelund, F., and E. Hansen (1967), A monograph on sediment transport in alluvial streams, *Technical University of Denmark 0stervoldgade 10, Copenhagen K.*

Federici, B., and G. Seminara (2006), Effect of suspended load on sandbar instability, *Water Resources Research*, *42*(7), 1–11, doi:10.1029/2005WR004399.

Ferguson, R. I., D. J. Bloomer, and M. Church (2011), Evolution of an advancing gravel front: Observations from Vedder Canal, British Columbia, *Earth Surface Processes and Landforms*, *36*(9), 1172–1182, doi:10.1002/esp.2142.

Fredsoe, J. (1978), Meandering and Braiding of Rivers, *Journal of Fluid Mechanics*, *84*(November), 609–624, doi:10.1017/S0022112078000373.

Fujita, Y., and Y. Muramoto (1982), Experimental Study on Stream Channel Processes in Alluvial Rivers, *Tech. Rep. 288*.

García, M. H., and Y. Niño (1993), Dynamics of sediment bars in straight and meandering channels: experiments on the resonance phenomenon, *Tech. Rep. January*, doi:10.1080/00221689309498815.

Garcia Lugo, G. A., W. Bertoldi, A. J. Henshaw, and A. M. Gurnell (2015), The effect of lateral confinement on gravel bed river morphology, *Water Resources Research*, *51*(9), 7145–7158, doi:10.1002/2015WR017081.

Hall, P. (2004), Alternating bar instabilities in unsteady channel flows over erodible beds, *Journal of Fluid Mechanics*, *499*(499), 49–73, doi:10.1017/S0022112003006219.

Ikeda, S. (1982), Prediction of alternate bar wavelength and height, *Saitama University Faculty of Engineering Construction Research Report*, (12), p23–45.

Ikeda, S. (1984), Prediction of Alternate Bar Wavelength and Height, *Journal of Hydraulic Engineering*, *110*(4), 371–386, doi:10.1061/(ASCE)0733-9429(1984)110:4(371).

Jaballah, M., B. Camenen, L. Pénard, and A. Paquier (2015), Alternate bar development in an alpine river following engineering works, *Advances in Water Resources*, *81*, 103–113, doi:10.1016/j.advwatres.2015.03.003.

Jaeggi, M. N. R. (1984), Formation and Effects of Alternate Bars, *Journal of Hydraulic Engineering*, *110*(2), 142–156, doi:10.1061/(ASCE)0733-9429(1984)110:2(142).

Jäggi, M. (1983), Mitteilungen der Versuchsanstalt für Wasserbau , Alternierende Kiesbanke, (62).

Jourdain, C., N. Claude, P. Tassi, F. Cordier, and G. Antoine (2020), Morphodynamics of alternate bars in the presence of riparian vegetation, *Earth Surface Processes and Landforms*, *45*(5), 1100–1122, doi:10.1002/esp.4776.

Kinoshita, R. (1961), Investigation of channel deformation in Ishikari River, *Report of Bureau of Resources, Dept. Science and Technology, Japan*, *174*.

Lanzoni, S. (2000), Experiments on bar formation in a straight flume: 1. Uniform sediment, *Water Resources Research*, *36*(11), 3337–3349, doi:10.1029/2000WR900160.

Lanzoni, S., and M. Tubino (1999), Grain sorting and bar instability, *Journal of Fluid Mechanics*, *393*, 149–174, doi:10.1017/S0022112099005583.

Meyer-Peter, E., and R. Muller (1948), Formulas for bed load transport, *Proceedings of the 2nd congress of the International Association for Hydraulic Research*, *2*, 39–64.

Muramoto, Y., and Y. Fujita (1978), The classification of meso-scale river bed configuration and the criterion of its formation, in *Proceedings of the Japanese Conference on Hydraulics*, vol. 22, pp. 275–282, Japan Society of Civil Engineers.

Nelson, J. M. (1990), The initial instability and finite-amplitude stability of alternate bars in straight channels, *Earth Science Reviews*, *29*(1-4), 97–115, doi:10.1016/0012-8252(0)90030-Y.

Nelson, P. A., and J. A. Morgan (2018), Flume experiments on flow and sediment supply controls on gravel bedform dynamics, *Geomorphology*, *323*, 98–105, doi:10.1016/j.geomorph.2018.09.011.

Paola, C. (2000), Quantitative models of sedimentary basin filling, *Sedimentology*, *47*, 121–178, doi:10.1046/j.1365-3091.2000.00006.x.

Parker, G. (1976), On the cause and characteristic scales of meandering and braiding in rivers, *Journal of Fluid Mechanics*, *76*(3), 457, doi:10.1017/S0022112076000748.

Parker, G. (1978), Self-formed straight rivers with equilibrium banks and mobile bed. Part 2. The gravel river, *Journal of Fluid Mechanics*, *89*(01), 127–146, doi:10.1017/S0022112078002505.

Parker, G. (1990), Surface-based bedload transport relation for gravel rivers, *Journal of Hydraulic Research*, *28*(4), 417–436, doi:10.1080/00221689009499058.

Parker, G., P. R. Wilcock, C. Paola, W. E. Dietrich, and J. Pitlick (2007), Physical basis for quasi-universal relations describing bankfull hydraulic geometry of single-thread gravel bed rivers, *Journal of Geophysical Research: Earth Surface*, *112*(4), 1–21, doi:10.1029/2006JF000549.

Qian, H., Z. Cao, H. Liu, and G. Pender (2017), Numerical modelling of alternate bar formation, development and sediment sorting in straight channels, *Earth Surface Processes and Landforms*, *42*(4), 555–574, doi:10.1002/esp.3988.

Ragno, N., M. Redolfi, and M. Tubino (2021), Coupled Morphodynamics of River Bifurcations and Confluences, *Water Resources Research*, *57*(1), 1–26, doi:10.1029/2020WR028515.

Redolfi, M., and M. Tubino (2014), A diffusive 1D model for the evolution of a braided network subject to varying sediment supply, in *River Flow 2014*, pp. 1153–1161, doi:10.1201/b17133-155.

Redolfi, M., G. Zolezzi, and M. Tubino (2016), Free instability of channel bifurcations and morphodynamic influence, *Journal of Fluid Mechanics*, *799*, 476–504, doi:10.1017/jfm.2016.389.

Redolfi, M., M. Welber, M. Carlin, M. Tubino, and W. Bertoldi (2020), Morphometric properties of alternate bars and water discharge: a laboratory investigation, *Earth*

Surface Dynamics, *8*(3), 789–808, doi:10.5194/esurf-8-789-2020.

Repetto, R., M. Tubino, and C. Paola (2002), Planimetric instability of channels with variable width, *Journal of Fluid Mechanics*, *457*, 79–109, doi:10.1017/S0022112001007595.

Rodrigues, S., E. Mosselman, N. Claude, C. L. Wintenberger, and P. Juge (2015), Alternate bars in a sandy gravel bed river: Generation, migration and interactions with superimposed dunes, *Earth Surface Processes and Landforms*, *40*(5), 610–628, doi:10.1002/esp.3657.

Seminara, G. (2010), Fluvial Sedimentary Patterns, *Annual Review of Fluid Mechanics*, *42*(1), 43–66, doi:10.1146/annurev-fluid-121108-145612.

Seminara, G., and M. Bolla Pittaluga (2012), Reductionist versus holistic approaches to the study of river meandering: An ideal dialogue, *Geomorphology*, *163-164*, 110–117, doi:10.1016/j.geomorph.2011.06.037.

Serlet, A. J., A. M. Gurnell, G. Zolezzi, G. Wharton, P. Belleudy, and C. Jourdain (2018), Biomorphodynamics of alternate bars in a channelized, regulated river: An integrated historical and modelling analysis, *Earth Surface Processes and Landforms*, *43*(9), 1739–1756, doi:10.1002/esp.4349.

Shaw, J. B., and B. McElroy (2016), Backwater number scaling of alluvial bed forms, *Journal of Geophysical Research: Earth Surface*, *121*, 1436–1455, doi:10.1002/2016JF003861.

Siviglia, A., G. Stecca, D. Vanzo, G. Zolezzi, E. F. Toro, and M. Tubino (2013), Numerical modelling of two-dimensional morphodynamics with applications to river bars and bifurcations, *Advances in Water Resources*, *52*, 243–260, doi:10.1016/j.advwatres.2012.11.010.

Struiksma, N., K. W. Olesen, C. Flokstra, and H. J. De Vriend (1985), Bed deformation in curved alluvial channels, *Journal of Hydraulic Research*, *23*(1), 57–79, doi:10.1080/00221688509499377.

Sukegawa, N. (1971), Study on meandering of streams in straight channels, *Report of Bureau of Resourcess, Dept. Science and Technology, Japan*, pp. 335–363.

Tharwat, A. (2018), Classification assessment methods, *Applied Computing and Informatics*, *17*(1), 168–192, doi:10.1016/j.aci.2018.08.003.

Tubino, M. (1991), Growth of alternate bars in unsteady flow, *Water Resources Research*, *27*(1), 37–52, doi:10.1029/90WR01699.

Tubino, M., and G. Seminara (1990), Free–forced interactions in developing meanders and suppression of free bars, *Journal of Fluid Mechanics*, *214*(4), 131–159, doi:10.1017/S0022112090000088.

Tubino, M., R. Repetto, and G. Zolezzi (1999), Free bars in rivers, *Journal of Hydraulic Research*, *37*(6), 759–775, doi:10.1080/00221689909498510.

Wilkinson, S. N., I. D. Rutherfurd, and R. J. Keller (2008), An experimental test of whether bar instability contributes to the formation, periodicity and maintenance of pool-riffle sequences, *Earth Surface Processes and Landforms*, *33*(11), 1742–1756, doi:10.1002/esp.1645.

Yalin, M. S., and A. M. F. Da Silva (2001), Fluvial processes, IAHR monograph, Delft: International Association for Hydraulic Research.